Performance Testing of APC Electric Fixed-Blade UAV Propellers

Or D. Dantsker* and Marco Caccamo †
Technical University of Munich, Garching, Germany

Robert W. Deters ‡
Embry-Riddle Aeronautical University - Worldwide, Daytona Beach, FL 32114

Michael S. Selig§
University of Illinois at Urbana–Champaign, Urbana, IL 61801

The increase in popularity of unmanned aerial vehicles (UAVs) has been driven by their use in civilian, education, government, and military applications. However, limited on-board energy storage significantly limits flight time and ultimately usability. The propulsion system plays a critical part in the overall energy consumption of the UAV; therefore, it is necessary to determine the most optimal combination of possible propulsion system components for a given mission profile, i.e., propellers, motors, and electronic speed controllers (ESC). Hundreds of options are available for the different components with little performance specifications available for most of them. APC Thin Electric propellers were identified as the most commonly used type of commercial-off-the-shelf propeller. However, little performance data exist in the open literature for the APC Thin Electric propellers with larger diameters. This paper describes the performance testing of 17 APC Thin Electric 2-bladed, fixed propellers with diameters of 12 to 21 in with various pitch values. The propellers were tested at rotation rates of 1,000 to 7,000 RPM and advancing flows of 8 to 80 ft/s, depending on the propeller and testing equipment limitations. Results are presented for the 17 propellers tested under static and advancing flow conditions with several key observations being discussed. The data produced will be available for download on the UIUC Propeller Data Site and on the Unmanned Aerial Vehicle Database.

Nomenclature

ESC	=	electronic speed controller	P	=	propeller power, propeller pitch
PWM	=	pulse width modulation	P/D	=	propeller pitch-to-diameter ratio
RPM	=	rotations per minute	Q	=	torque
UAV	=	unmanned aerial vehicle	R	=	universal gas constant
			Re	=	Reynolds number
c	=	chord	T	=	thrust, ambient temperature
C_P	=	power coefficient	V	=	flow speed
C_T	=	thrust coefficient			
D	=	propeller diameter	η	=	propeller efficiency
J	=	advance ratio	μ	=	viscosity
n	=	propeller rotation rate	ρ	=	density of air
p	=	ambient pressure			

*Researcher, School of Engineering and Design, or.dantsker@tum.de
†Professor, School of Engineering and Design, mcaccamo@tum.de
‡Associate Professor, Department of Engineering and Technology, AIAA Member. detersr1@erau.edu
§Professor Emeritus, Department of Aerospace Engineering, AIAA Associate Fellow. m-selig@illinois.edu

I. Introduction

In recent years, there has been an uptrend in the popularity of UAVs driven by the desire to apply these aircraft to areas such as precision farming, infrastructure and environment monitoring, surveillance, surveying and mapping, search and rescue missions, weather forecasting, and more. A key design constraint among unmanned aircraft has been energy storage, which significantly limits flight time and ultimately usability. The critical choice in UAV development then becomes what type of propulsion system to use. A mission-based propulsion system optimization tool was developed[1] to select the most optimal combination of possible propulsion system components for a given mission profile, i.e., propellers, motors, and ESCs.

Currently, there are hundreds of propeller and dozens of motor and ESC options in the radio control model market for small- to medium-sized airframes (1-3 m wingspans), yielding thousands of possible choices. Therefore, the problem becomes gathering component parameters with often scarce performance specifications. Based on examination of existing mid-sized electric unmanned aircraft, APC-E[2] fixed-blade electric propellers were identified as good candidates as these propellers are well known in the UAV industry to offer superior performance and are ubiquitous.

Previous propeller testing efforts by the authors have measured mostly smaller (less than 12 in diameter) electric fixed-blade propellers from APC as well as those from other manufacturers such as Master Airscrew, AeroNaut, Graupner, Kavan, etc.[3,4] However, there exists little performance data for larger propeller with diameters of 12 to 21 in. Figure 1 shows the profile of an APC 13x8 E fixed-blade electric propeller, which is provides a good representation of the propeller geometry typical for the APC Thin Electric propellers, in the tested size range.

Other works have measured the performance and efficiency parameters of propellers as well as other electric UAV propulsion system components. Brandt[5,6] and Uhlig[7,8] explored the performance of low Reynolds number propellers at slow speeds and past stall. Lundstrom performed a similar test using an automotive-based testing rig.[9,10] Deters looked into the performance of micro propellers for both small/micro air vehicles,[11,12] later expanding the work to examine static performance of micro propellers for quadrotors.[13,14] Lindahl[15] tested large UAV propellers in a wind tunnel while Chaney[16] and Dantsker[17] did so using automotive based rigs. Lindahl also tested the effects of using different motors with a given propeller. Drela has done extensive work testing and modelling motors and propellers.[18–20] Green[21] and Gong[22] have modelled and tested the efficiency of ESCs. Gong has also tested a propeller-motor combination in a wind tunnel[23] as well as create an in-flight thrust measurement system.[24]

This paper describes the performance testing of 17 APC Thin Electric 2-bladed, fixed propellers with diameters of 12 to 21 in. with various pitch values. The paper first presents the experimental methodology, including the equipment, testing procedure, calibration, data reduction, and wind tunnel corrections. Results and discussion are then given including the performance results for the 17 propellers for static and advancing flow conditions. Finally, a summary and statement of future work is given.

Figure 1: A photo of a APC 13x8 E propeller.

Experimental Methodology

A. Equipment

Propeller tests were conducted in the UIUC low-turbulence subsonic wind tunnel. The wind tunnel is an open-return type with a 7.5:1 contraction ratio. The rectangular test section is 2.8×4.0 ft (0.853×1.22 m) in cross section and 8-ft (2.44-m) long. To account for the boundary-layer growth at the side wall, the width increases by approximately 0.5 in. (1.27 cm) over the length of the test section. In order to have low turbulence levels at the test section, a 4-in. (10.2-cm) honeycomb and four anti-turbulence screens are in the settling chamber. The resulting turbulence intensity for an empty tunnel has been measured to be less than 0.1%.[25] A 125-hp (93.2-kW) AC motor driving a five-bladed fan is used to control the test-section speed up to 160 mph (71.5 m/s). The maximum test-section speed for these tests was 80 ft/s (24.4 m/s). Test-section speeds were measured using a MKS differential pressure transducer connected to static ports at the settling chamber and at the beginning of the test section. For test-section speeds below 40 ft/s (12.2 m/s), a MKS 220 1-torr transducer was used, and for speeds greater than 40 ft/s (12.2 m/s), a MKS 221 10-torr transducer was used. Ambient pressure was measured using a Setra Model 270 pressure transducer, and ambient temperature was measured using an Omega GTMQSS thermocouple.

Propeller performance was measured using the thrust and torque balance shown in Fig. 2. Thrust was measured outside of the tunnel test section using a T-shaped pendulum balance that pivoted about two flexural pivots and was constrained on one side by a load cell.[5] The Interface SMT S-Type load cell with a load capacity of 25 lb (110 N) and the Interface SMT S-Type load cell with a load capacity of 50 lb (220 N) were used. The balance was designed to allow the load cell to be placed in 10 different locations in order to use the full range of the load cell based on the thrust produced. The load cell locations ranged from 3.25 in (8.26 cm) from the pivot point to 7.75 in (19.69 cm) in 0.5-in (1.27-cm) increments. A preload weight was added to the balance on the opposite side to the load cell. This preload weight kept the load cell in tension during all aspects of testing to make sure the load cell would not slip during negative thrust conditions.

The torque from the propeller was measured using a reaction torque sensor (RTS) transducer from Transducer Techniques with capacity of either 100 or 200 oz-in (0.708 N-m or 1.416 N-m). The torque cell was placed between the motor sting and the support arm of the thrust balance. To remove the torque cell, motor sting, balance support arm, and any wires from the propeller slipstream and test section velocity, a fairing surrounded the setup as shown in Fig. 3. The fairing spanned the test section from the floor to the ceiling in order to keep the test section flow symmetric. The motor sting was long enough for all the propellers to be more than 1.5 diameters ahead of the fairing in order to minimize the effect of the fairing on the propeller performance.

Propeller RPM was measured by shining a red laser with a wavelength of 630-680 nm through the propeller disc area to a phototransistor with a rise time of 5 μsec. The output from the phototransistor is amplified so that the maximum voltage when the laser shines on the receiver is over 2 V. As the propeller spins, the propeller blades block the laser beam, and the receiver output voltage drops to around zero. Each time the propeller RPM was measured, the voltage was recorded at 40,000 Hz for 30,000 samples. The high rate and sample number is so that the resulting square wave is captured and the voltage peaks can be counted. The RPM was calculated by dividing the number of peaks by the sample time and by the number of propeller blades. The phototransistor rise time and the sample rate have been more than sufficient in finding the typical RPM values for the propellers tested. This measurement technique was compared to results from a handheld digital tachometer, and the results agreed.

During the tests, the propellers were driven by the Hacker A40-14L V4 14-pole (355 kV) brushless motor using a Castle Creations Edge 75 speed controller. To simplify the laboratory setup, a 1.5 kW power supply by MEAN WELL was used to power the motor and speed controller. To set the rotational speed of the motor, the speed controller

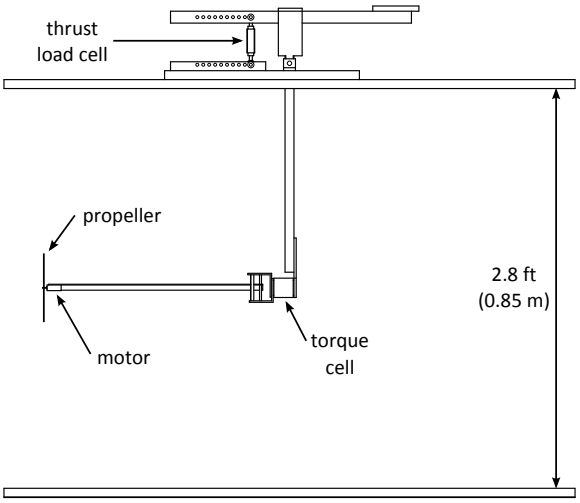

Figure 2: Propeller thrust and torque balance.

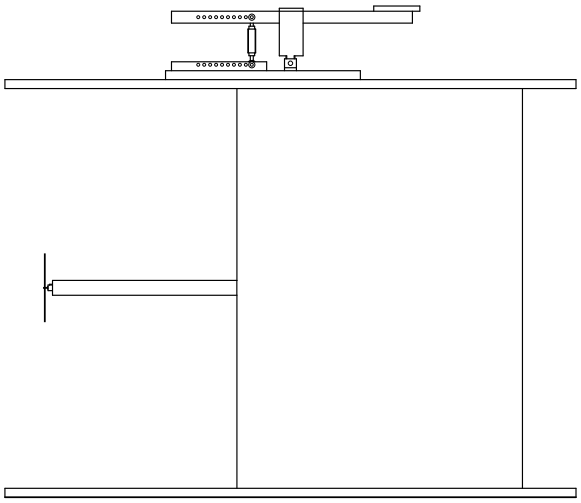

Figure 3: Propeller balance enclosed in fairing.

was connected to a modified ServoXciter EF from Vexa Control. While designed to test RC servos by adjusting the pulse-width signal to the servo, the ServoXciter also works well as the throttle for the motor. A voltage from the computer would be sent to ServoXciter, and in turn the ServoXciter would then send a pulse-width signal to the speed controller to control the motor speed.

B. Testing Procedure

All voltages from the testing equipment were recorded by a National Instruments PCI-6031E 16-bit analog-to-digital data acquisition (DAQ) board connected to a personal computer. The DAQ board is capable of measuring 32 differential analog inputs simultaneously at a maximum sample rate of 100 kS/s. As mentioned earlier, propeller RPM measurements were recorded at 40,000 Hz for 30,000 samples. This high sample rate required the RPM measurement to be taken separately from the rest of the measurements. All other measurements (thrust, torque, dynamic pressure, atmospheric pressure, and temperature) were taken simultaneously immediately afterwards at a rate of 3,000 Hz for 3,000 samples. This method has been more than sufficient as differences in motor speed have been observed to change less than 1% during these time periods. A LabVIEW® program was written to read the DAQ board as well as control the motor speed and wind tunnel speed.

For static performance tests, the propeller thrust and torque were measured along with the ambient pressure and temperature at different RPM values. For advancing flow performance tests, the propeller RPM was set and the tunnel speed was increased from 8 ft/s to 40 ft/s by 2 ft/s increments. During this test, a MKS 1-torr pressure transducer was used to measure the tunnel speed. At each velocity, the propeller thrust and torque were measured along with the tunnel speed and ambient pressure and temperature. If the torque value became too close to zero, the test was stopped because the propeller was approaching the windmill brake state. If the propeller reached 40 ft/s before the windmill brake state was achieved, the same RPM was used for tunnel speeds of 34 ft/s to 80 ft/s by 2 ft/s increments using a MKS 10-torr transducer to measure the tunnel speed. Again the test would stop early if the propeller was close to windmilling. The overlap with the 1-torr and 10-torr tests were to ensure consistent data between low and high speed tests. Typically at least three RPM values were tested to document Reynolds number effects.

C. Calibration

Since the DAQ board only records voltages from the transducers and load cells, each voltage is converted to a physical measurement through calibration curves. The pressure transducer that measured the ambient pressure and the thermocouple that measured ambient temperature used manufacturer supplied calibration equations to convert the voltages to pressure and temperature. The MKS differential pressure transducers used to measure tunnel pressures also used manufacturer calibration slopes.

The load and torque cells do not use manufacturer supplied calibration values. Instead the calibration slopes are found during testing. Thrust calibration used precisely measured weights and a pulley system to represent a thrust on the load cell. By increasing and decreasing a known force on the load cell, a linear relationship between the thrust and voltage was calculated. For torque calibration, the precision weights were applied to a moment arm to create a known torque. By increasing and decreasing this torque, a linear relationship between the torque and voltage was calculated. These calibration procedures were performed regularly to ensure consistent results, and any change in the slopes were typically 1% or less.

D. Data Reduction

As mentioned in Section A, the ambient pressure and temperature were measured using a pressure transducer and thermocouple, respectively. Air density was then calculated from the equation of state

$$p = \rho RT \tag{1}$$

where R is the universal gas constant. The standard value of 1716 $\mathrm{ft}^2/\mathrm{s}^2/^\circ\mathrm{R}$ (287.0 $\mathrm{m}^2/\mathrm{s}^2/\mathrm{K}$) for air was used.

Propeller power is calculated from the measured propeller torque by

$$P = 2\pi nQ \tag{2}$$

Performance of a propeller is typically given in terms of the thrust and power coefficients, defined as

$$C_T = \frac{T}{\rho n^2 D^4} \tag{3}$$

$$C_P = \frac{P}{\rho n^3 D^5} \tag{4}$$

where nD can be considered the reference velocity and D^2 can be considered the reference area. When the propeller is in a freestream flow, the advance ratio is defined in terms of the velocity and the rotation rate.

$$J = \frac{V}{nD} \tag{5}$$

The efficiency of a propeller is a measure of the useful power (TV) divided by the input power (P).

$$\eta = \frac{TV}{P} \tag{6}$$

Putting the efficiency in term of C_T, C_P, and J yields

$$\eta = \frac{C_T J}{C_P} \tag{7}$$

E. Wind Tunnel Corrections

Two wind tunnel corrections were used to account for the effects of testing a propeller in front of a fairing and in a closed test section. Since the propellers are tested on a string in front of a fairing, the air velocity seen by the propellers will be less than the velocity measured at the begining of the test section. To account for this lower velocity, a velocity correction factor was developed based on the propeller size and its distance from the fairing.

Since the fairing spanned the test section from the floor to ceiling, the fairing was modeled as an airfoil using source panels. In order to satisfy the boundary condition of no cross flow at the tunnel side walls, reflections of the airfoil were included. The strength of each source panel and the flowfield surrounding the airfoil was then found using the method described in Anderson.[26] Using 100 sets of reflection pairs, the cross flow at the tunnel side walls was found to be less than $2 \times 10^{-6}\%$ of the freestream. The resulting 2D flowfield from the source panels was assumed to be the same along the span of the fairing. The propeller size is small compared to the height of the tunnel, so any wall effects from the floor and ceiling were assumed to be negligible. Since the propeller will see different corrected velocities along its disk area, a weighted average was used to calculate a single velocity reduction factor $k_{fairing}$ (Eq. 8).

$$\frac{V_{c_{fairing}}}{V_\infty} = k_{fairing} \tag{8}$$

In order to simplify the calculations needed during testing, a series of correction factors were tabulated beforehand covering the full range of propeller sizes and locations. During a test, the correction factor was found by interpolation using the current propeller size and location.

To account for testing a propeller in a closed test section, the classic Glauert[27,28] correction was used. The flow around a propeller in a closed test section is different than the flow in free air. For a propeller producing thrust, the velocity in the propeller slipstream is greater than the nominal test section velocity. Since the same volume of air must pass ahead of the propeller as it does behind the propeller from continuity, the velocity outside of the slipstream must be lower. The pressure outside of the slipstream is also higher than the pressure ahead of the propeller, so the thrust measured is larger than the thrust produced at the same velocity in free air. Another way to describe the results is that the thrust measured would occur at a lower velocity in free air. To determine that lower velocity, the correction factor is found from

$$\frac{V_c}{V_\infty} = 1 - \frac{\tau\alpha}{2\sqrt{1+2\tau}} \tag{9}$$

where $\tau = T/\rho A V_\infty^2$ and $\alpha = A/C$. This correction is the first approximation of the iterative method described by Glauert, but for the propeller sizes, thrust values, and freestream speeds from this series of tests, the correction factor from Eq. 9 agrees with the full iterative method to a difference of less than 1%.

II. Results and Discussion

A total of 17 APC Thin Electric "APC-E" 2-bladed, fixed propellers with diameters from 12 to 21 inches, were tested in static conditions (no-freestream) and in advancing flow in the wind tunnel. Table 1 lists the specific diameters and pitches for the propellers that were tested. The static and wind tunnel performance data of these propellers are presented in Figs. 4–37. This data will be available for download on the UIUC Propeller Data Site[3] and on the Unmanned Aerial Vehicle Database.[29] During the testing and after examining the reduced data, several trends were noted and these are discussed next.

First, it is important to note that all of the propellers tested were purchased between 2019 and 2021. The authors have noted differences between the current APC propellers tested and propellers purchased in the early 2000s with the identical size (diameter and pitch) and type marking (Thin Electric indicated by a "E"). These differences include propeller color, regions of blade transparency when held up to a light source, and hub thickness difference. It is suspected that the specific material formulation used to injection mold the propellers, i.e. glass fibers within a Nylon matrix and the design of the propeller hub, has changed over the years. The latter suspicion (hub redesign) has been confirmed by APC on their website, occurring in 2010; this change is said to make the propellers more robust, quieter, and more efficient at higher RPM conditions by slightly thickening the hub and hub-to-blade transition.[2]

Next, through visual observation, propellers with the same diameter but different pitch numbers had very similar blade geometries. Specifically, the chord at each station is approximately identical between propellers with the same diameter but different pitch numbers. The difference between propellers of the same diameter is the blade twist distributions, which is required to achieve the variation in pitch values.

Through performance testing, it was observed that with increasing pitch for a given propeller diameter, the thrust, power, and efficiency coefficient curves shift up and to the right. This observation correlates to increasing pitch-to-diameter (P/D) ratio of a propeller with greater values of thrust, power, and efficiency coefficients at greater advance ratios; this general trend is expected. It should be noted that the performance curves for propellers with high P/D ratios are incomplete because of the 80 ft/s speed limitation set by the structural design of the propeller balance fairing. Likewise, as expected, as pitch increases for a given propeller diameter, the static (zero velocity) thrust and power coefficients increases.

Table 1: List of APC-E Thin Electric Propellers Tested

APC-E Propellers Categorized by Diameter						
APC-E 12×6	APC-E 13×6.5	APC-E 14×7	APC-E 16×6	APC-E 18×8	APC-E 20×10	APC-E 21×13
APC-E 12×8	APC-E 13×8	APC-E 14×8.5	APC-E 16×8	APC-E 18×10		
APC-E 12×10	APC-E 13×10	APC-E 14×10	APC-E 16×10	APC-E 18×12		

APC 12×6 Thin Electric Propeller

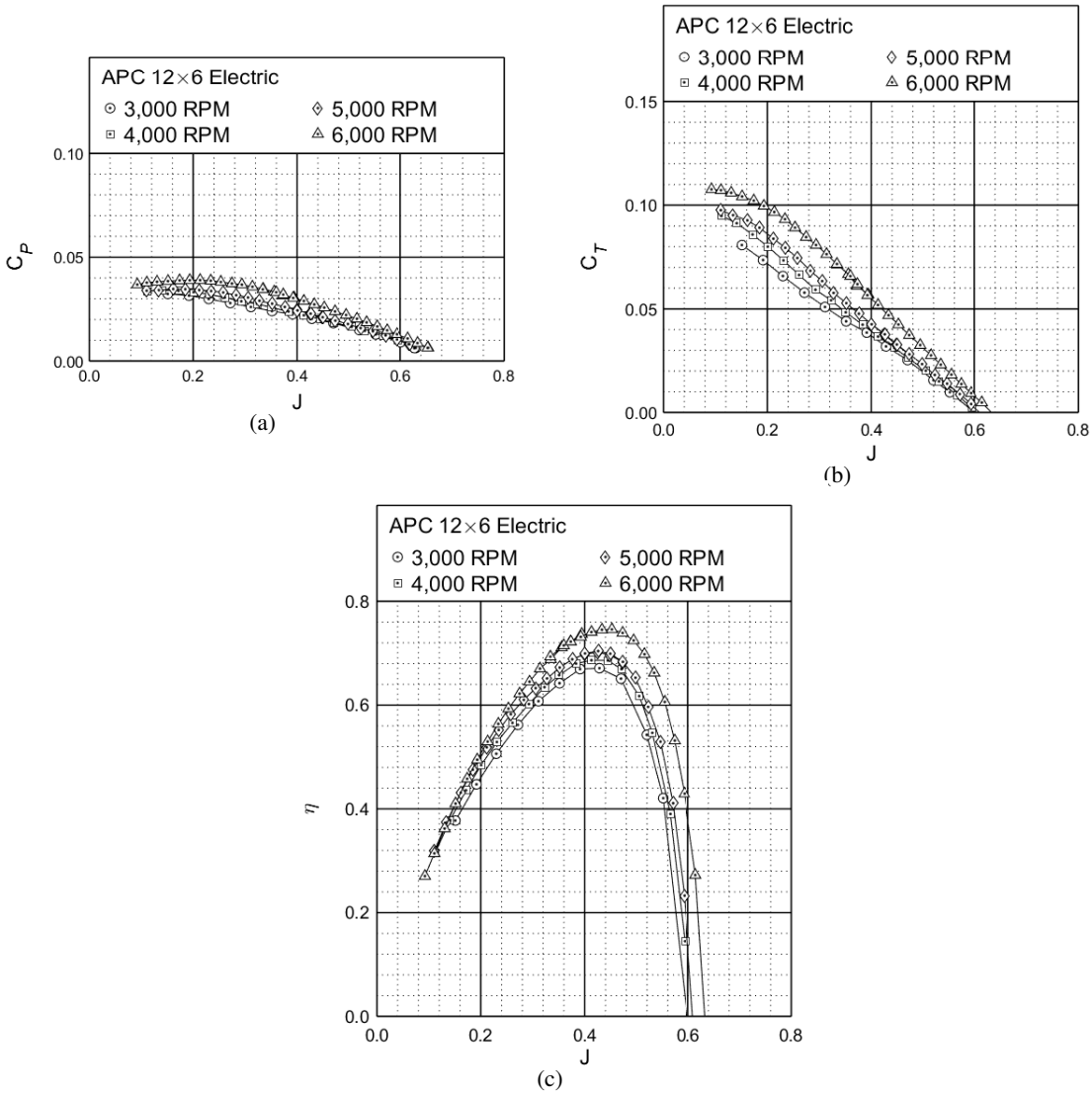

Figure 4: Performance of the APC 12×6 Thin Electric propeller: (a) thrust coefficient, (b) power coefficient, (c) efficiency.

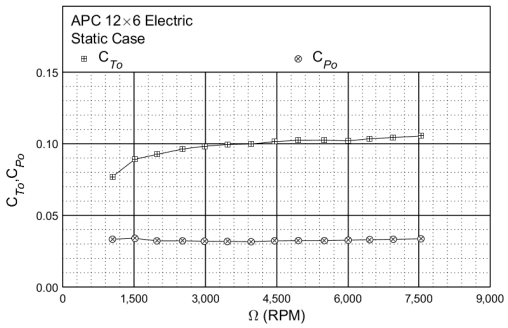

Figure 5: Static performance of the APC 12×6 Thin Electric propeller: thrust and power coefficient.

APC 12×8 Thin Electric Propeller

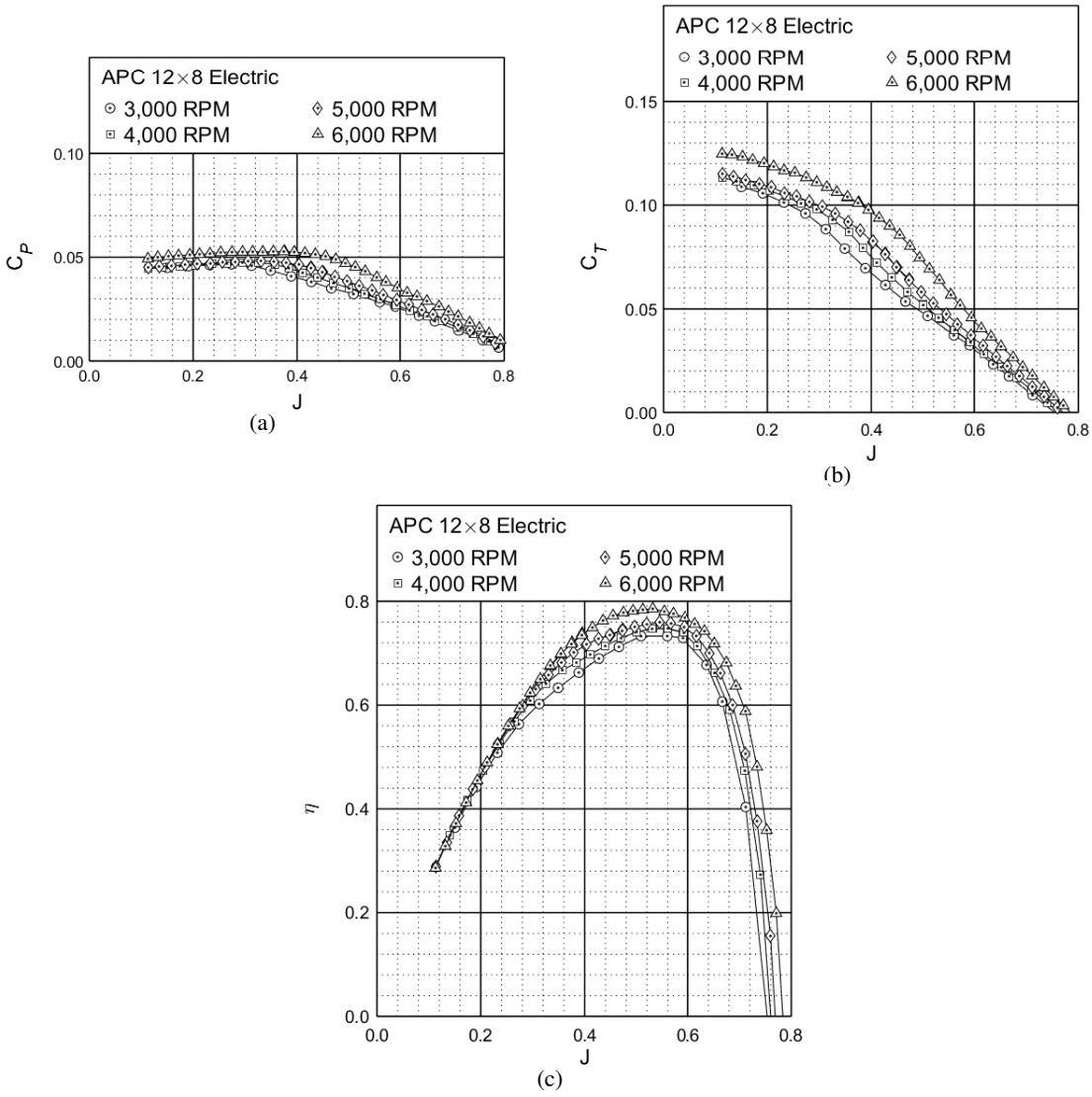

Figure 6: Performance of the APC 12×8 Thin Electric propeller: (a) thrust coefficient, (b) power coefficient, (c) efficiency.

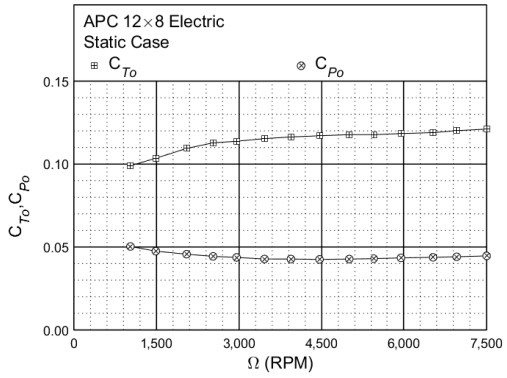

Figure 7: Static performance of the APC 12×8 Thin Electric propeller: thrust and power coefficient.

APC 12×10 Thin Electric Propeller

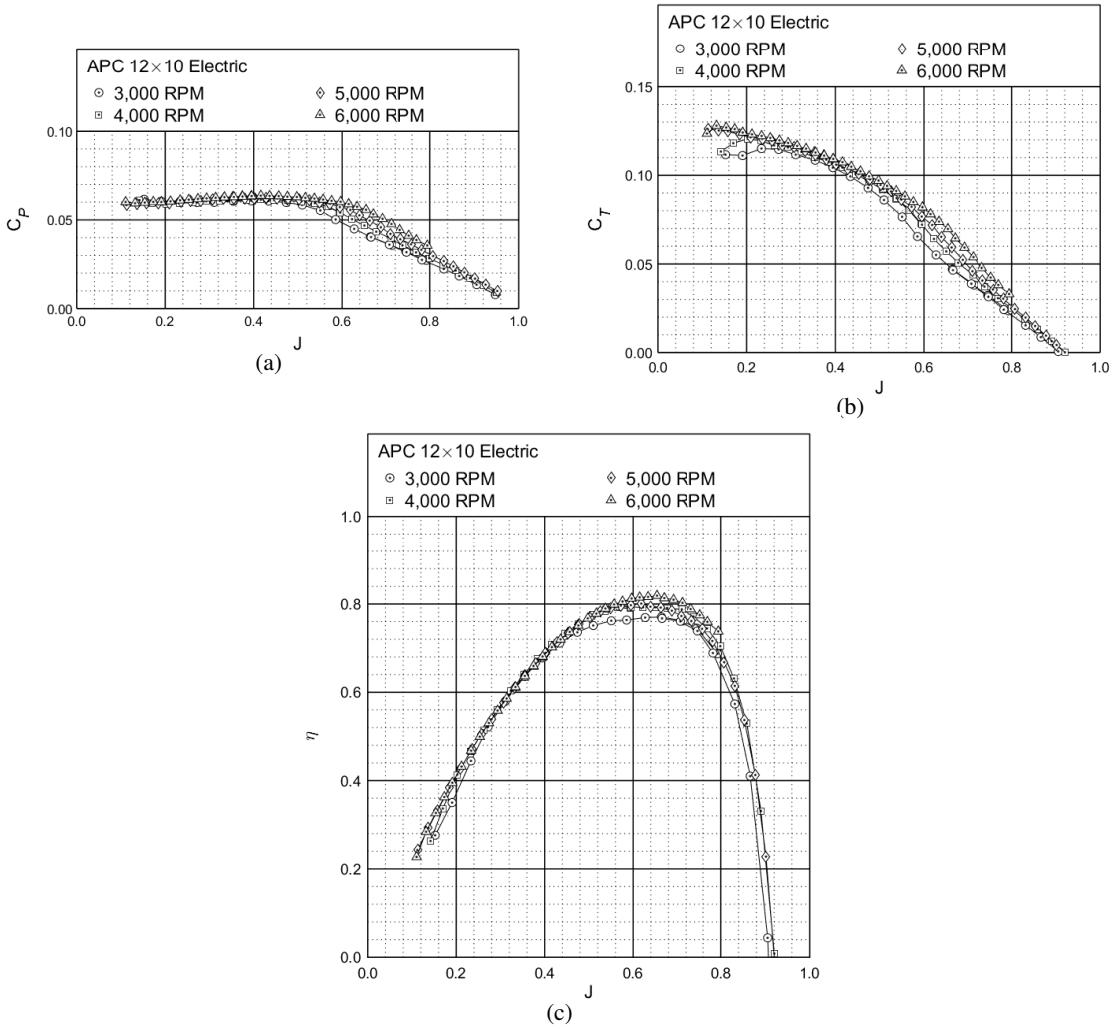

Figure 8: Performance of the APC 12×10 Thin Electric propeller: (a) thrust coefficient, (b) power coefficient, (c) efficiency.

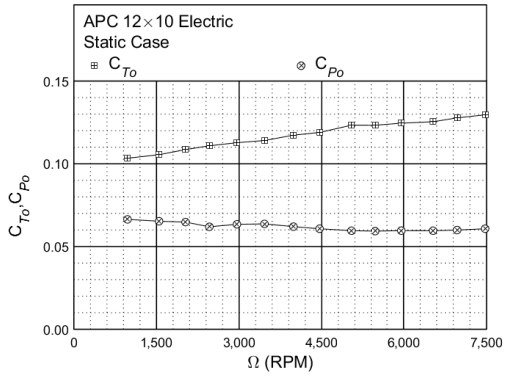

Figure 9: Static performance of the APC 12×10 Thin Electric propeller: thrust and power coefficient.

APC 13×6.5 Thin Electric Propeller

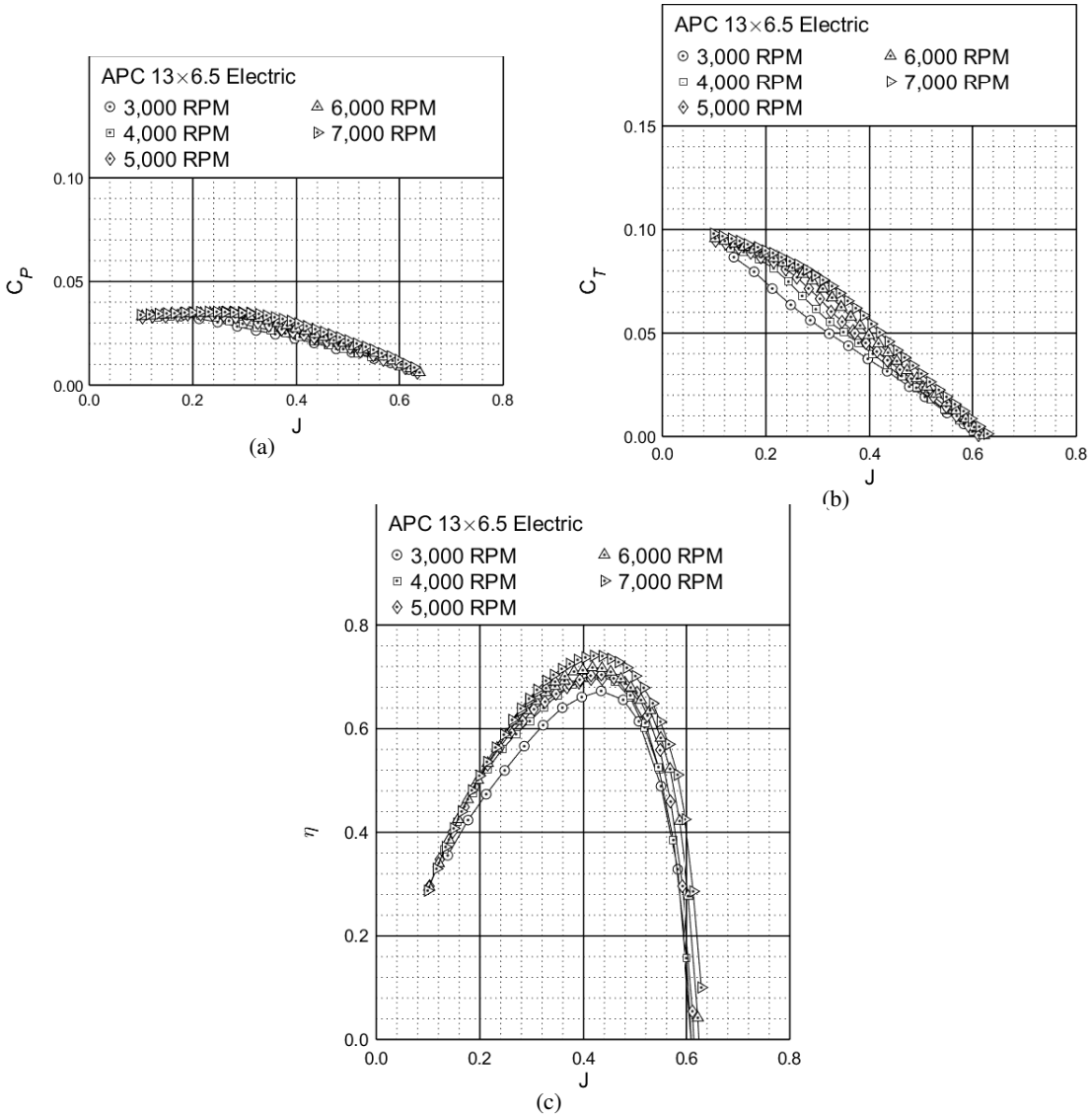

Figure 10: Performance of the APC 13×6.5 Thin Electric propeller: (a) thrust coefficient, (b) power coefficient, (c) efficiency.

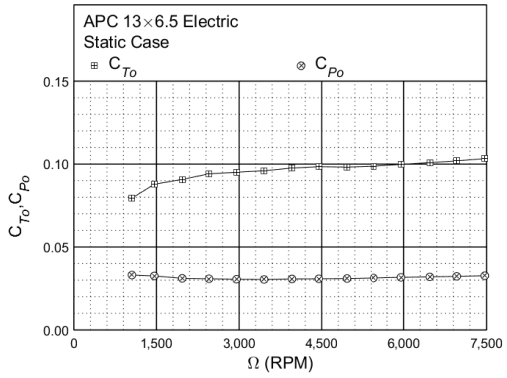

Figure 11: Static performance of the APC 13×6.5 Thin Electric propeller: thrust and power coefficient.

APC 13×8 Thin Electric Propeller

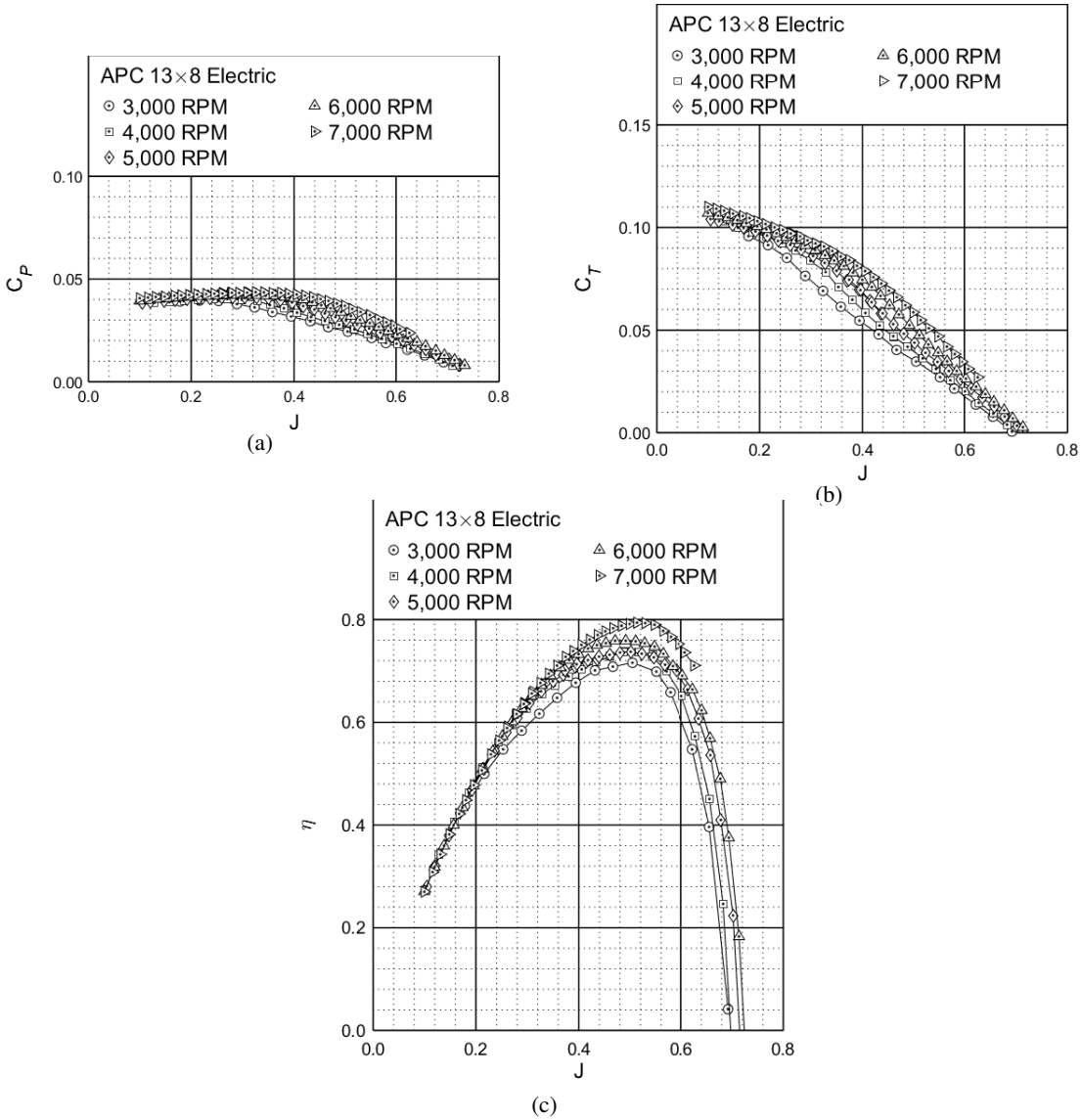

Figure 12: Performance of the APC 13×8 Thin Electric propeller: (a) thrust coefficient, (b) power coefficient, (c) efficiency.

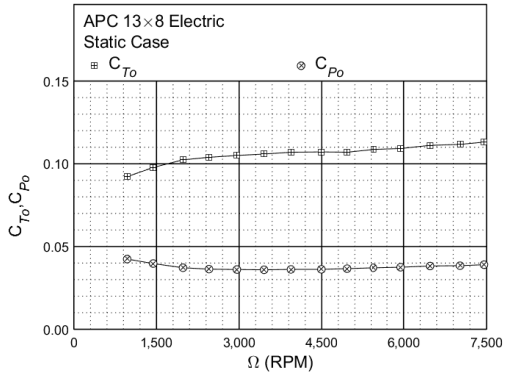

Figure 13: Static performance of the APC 13×8 Thin Electric propeller: thrust and power coefficient.

APC 13×10 Thin Electric Propeller

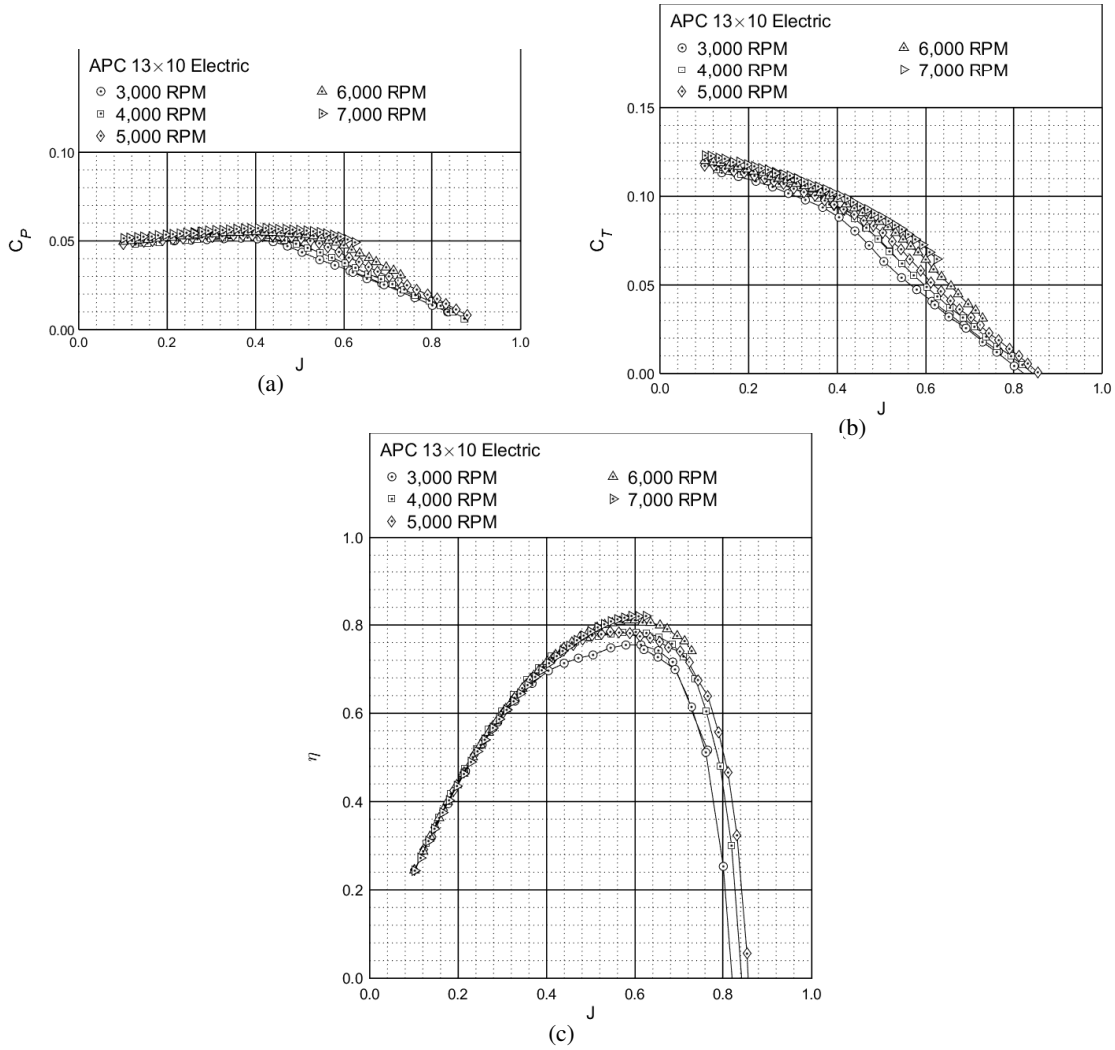

Figure 14: Performance of the APC 13×10 Thin Electric propeller: (a) thrust coefficient, (b) power coefficient, (c) efficiency.

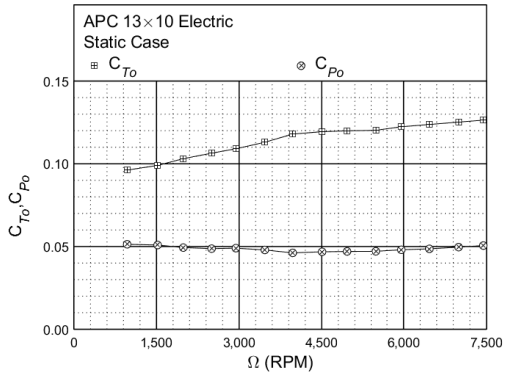

Figure 15: Static performance of the APC 13×10 Thin Electric propeller: thrust and power coefficient.

APC 14×7 Thin Electric Propeller

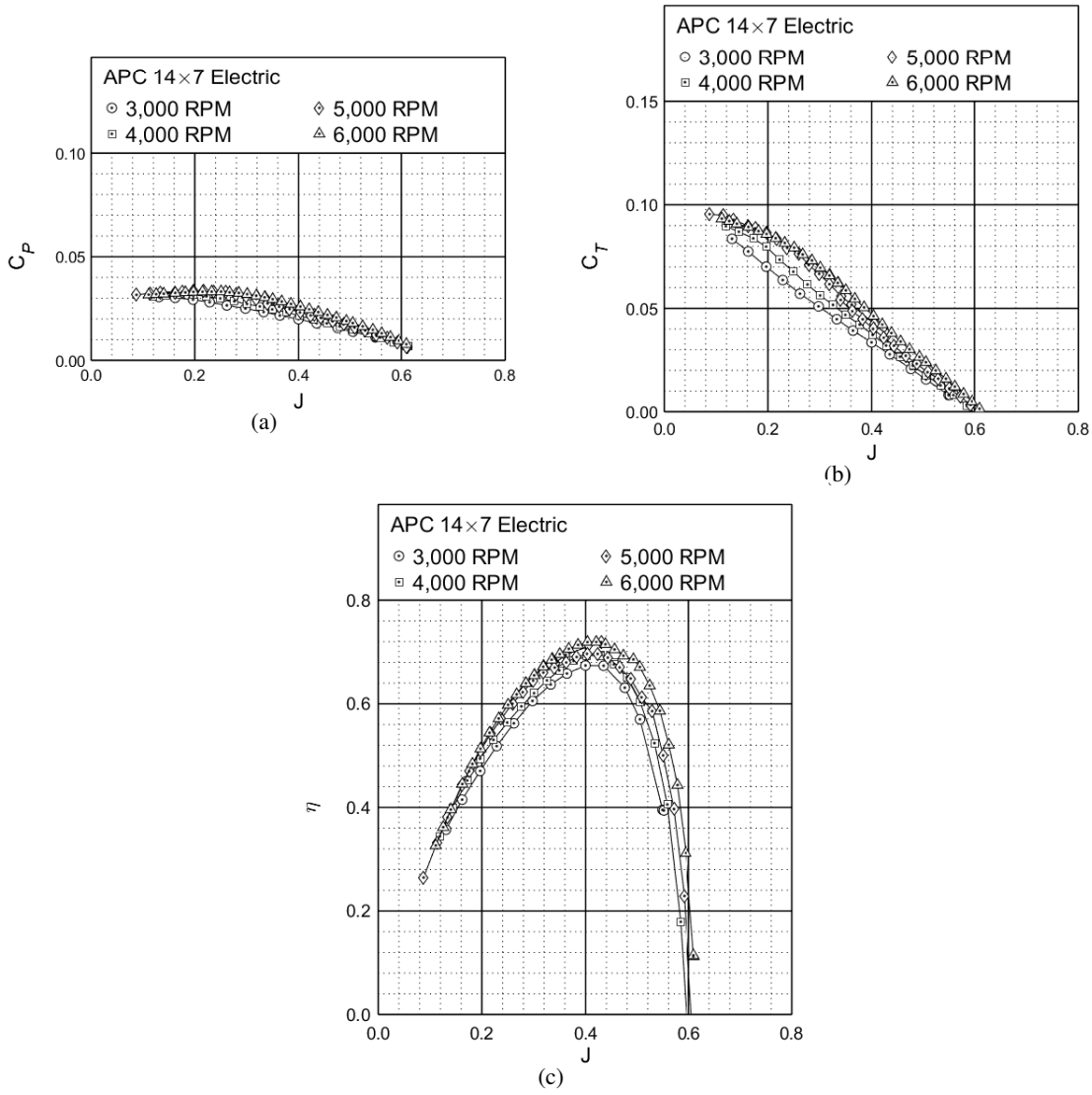

Figure 16: Performance of the APC 14×7 Thin Electric propeller: (a) thrust coefficient, (b) power coefficient, (c) efficiency.

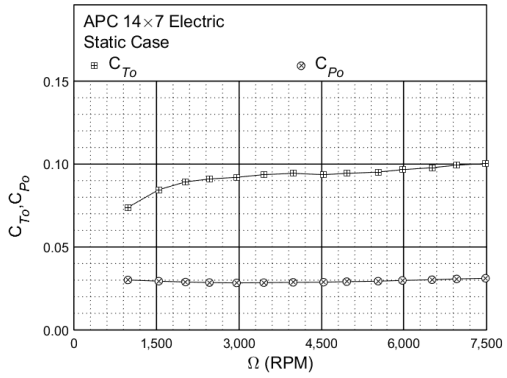

Figure 17: Static performance of the APC 14×7 Thin Electric propeller: thrust and power coefficient.

APC 14×8.5 Thin Electric Propeller

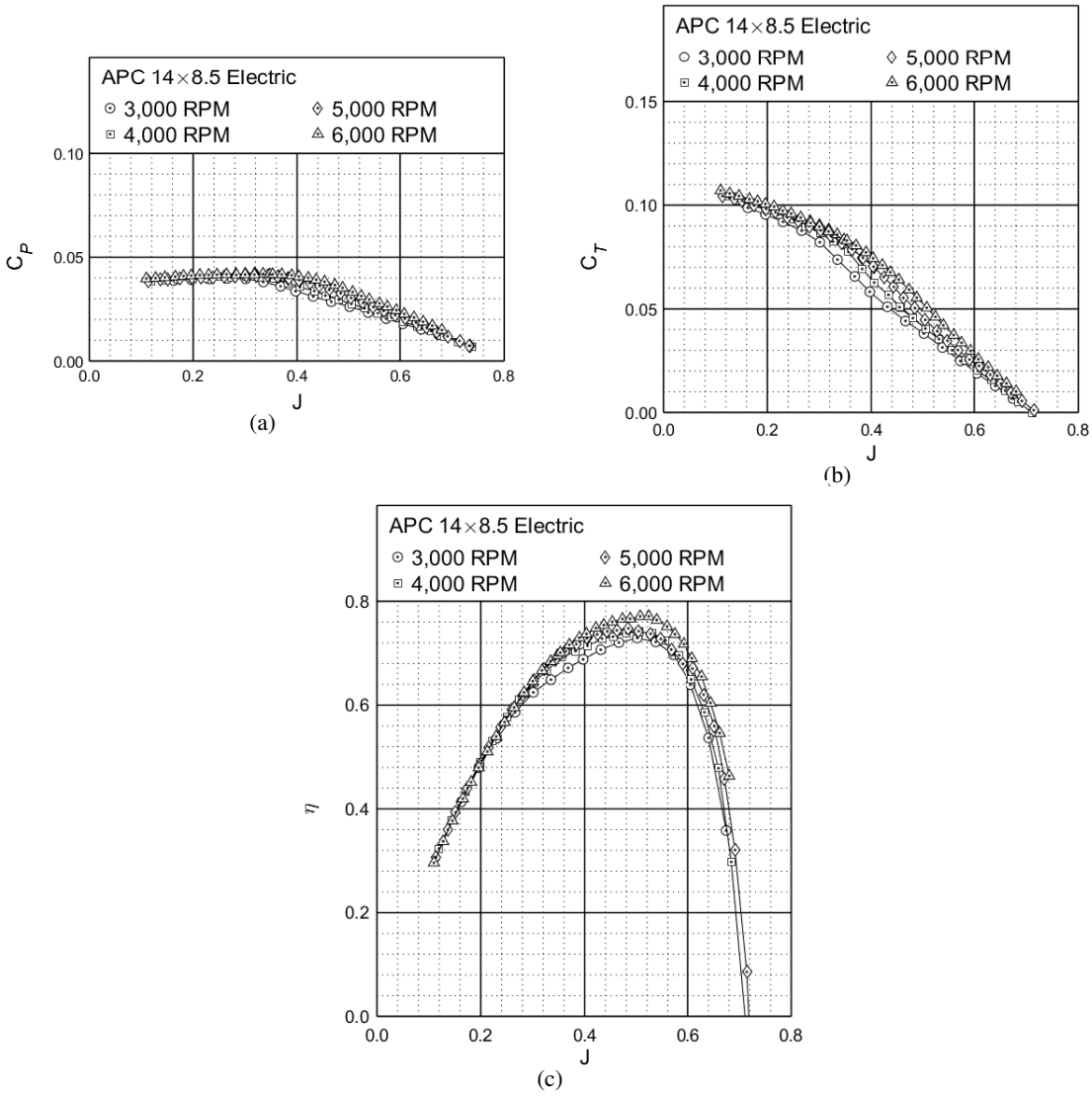

Figure 18: Performance of the APC 14×8.5 Thin Electric propeller: (a) thrust coefficient, (b) power coefficient, (c) efficiency.

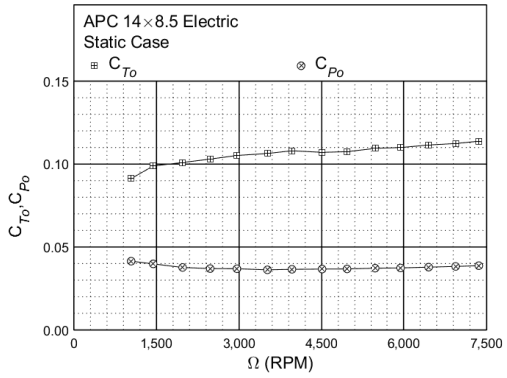

Figure 19: Static performance of the APC 14×8.5 Thin Electric propeller: thrust and power coefficient.

APC 14×10 Thin Electric Propeller

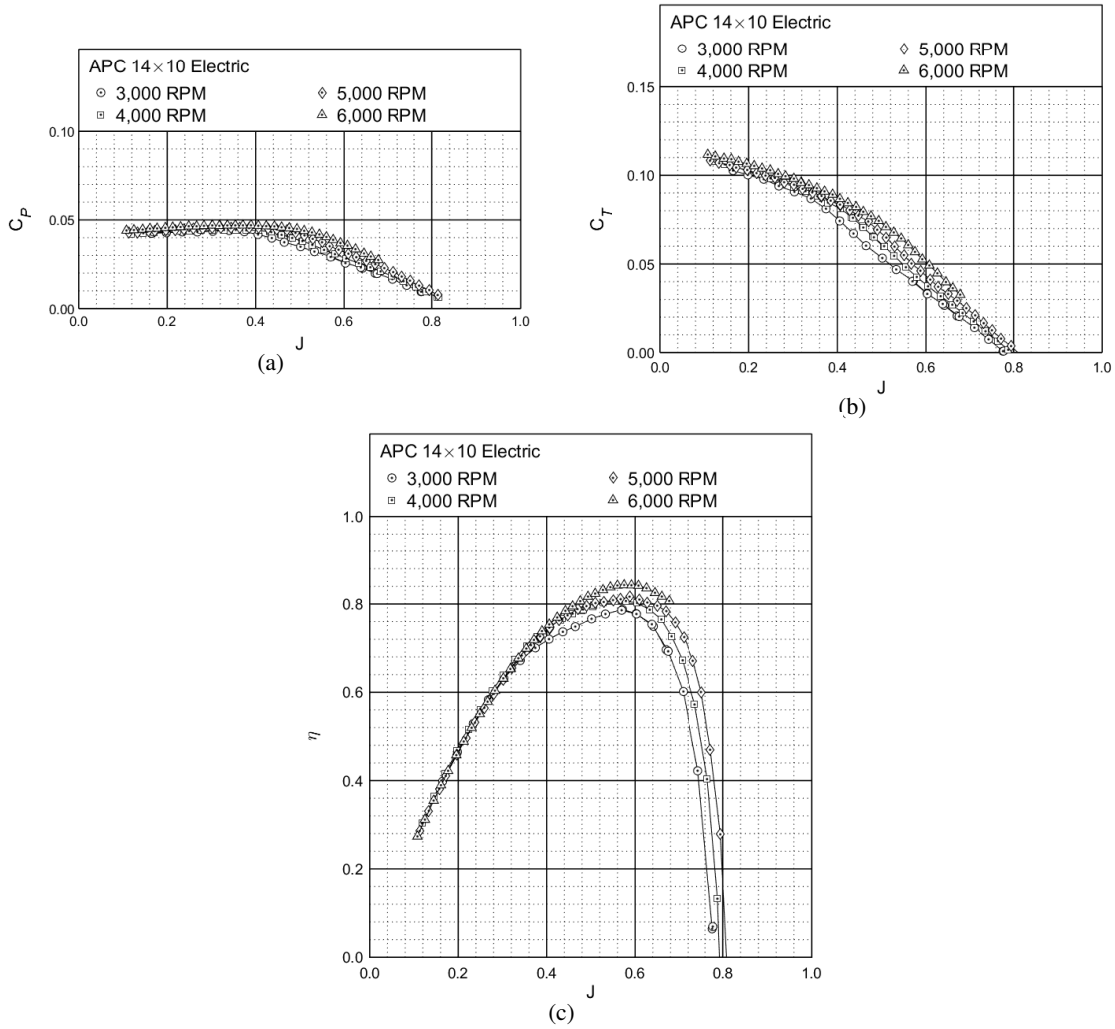

Figure 20: Performance of the APC 14×10 Thin Electric propeller: (a) thrust coefficient, (b) power coefficient, (c) efficiency.

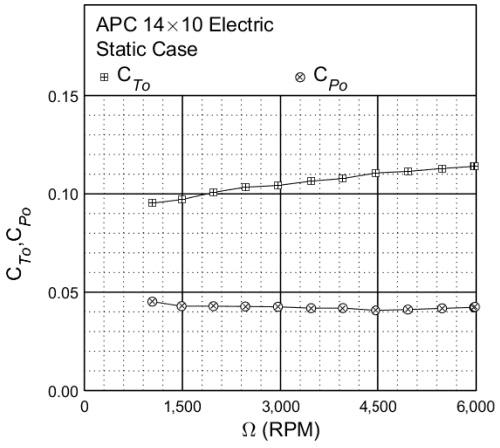

Figure 21: Static performance of the APC 14×10 Thin Electric propeller: thrust and power coefficient.

APC 16×8 Thin Electric Propeller

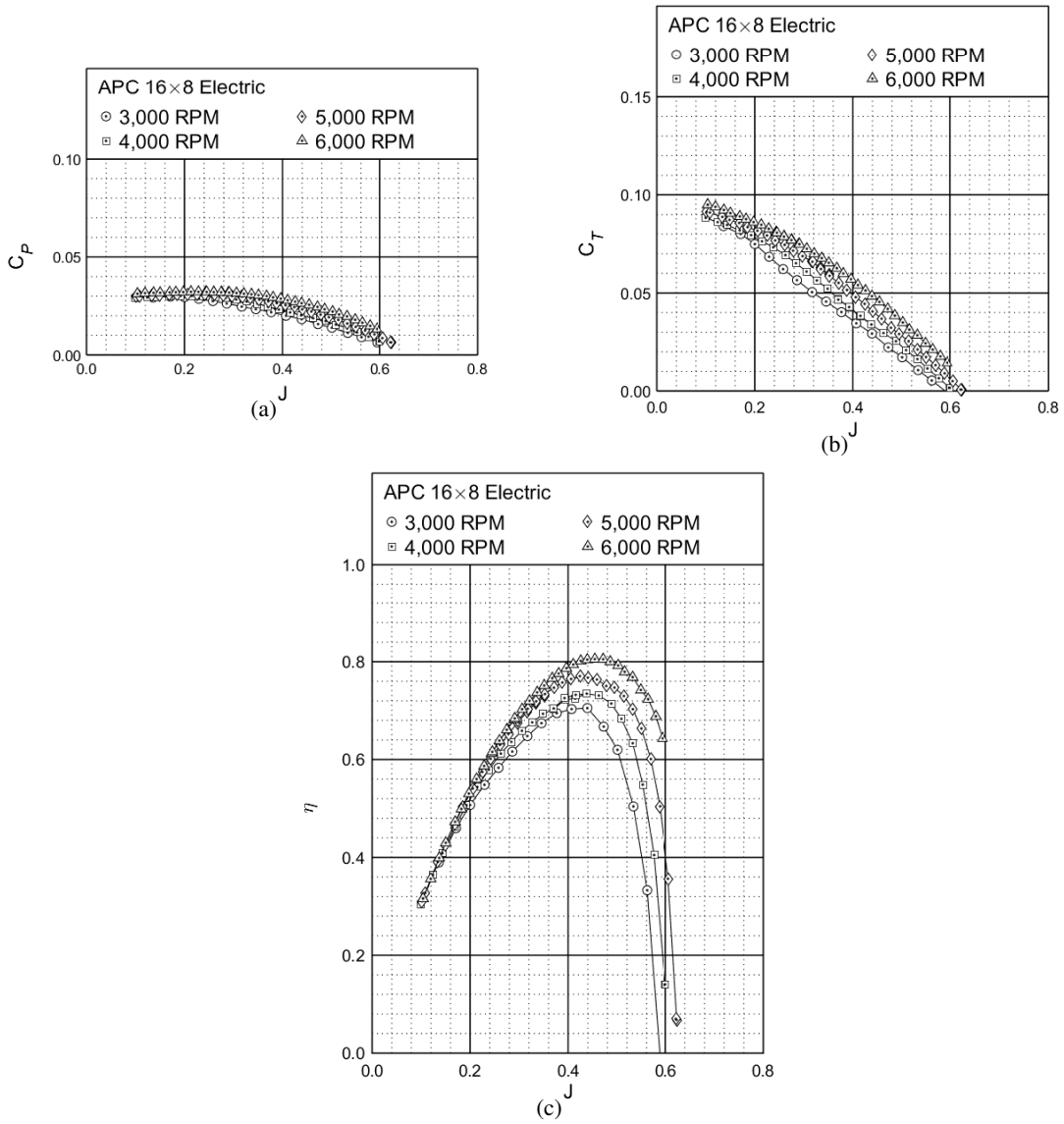

Figure 22: Performance of the APC 16×8 Thin Electric propeller: (a) thrust coefficient, (b) power coefficient, (c) efficiency.

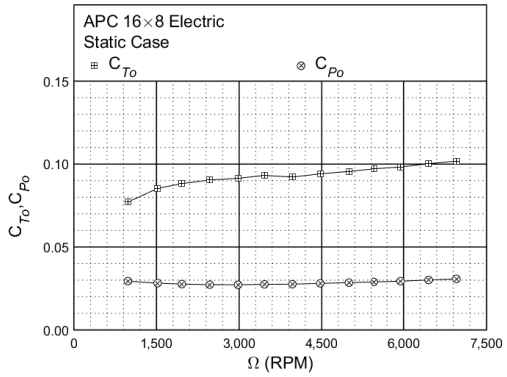

Figure 23: Static performance of the APC 16×8 Thin Electric propeller: thrust and power coefficient.

APC 16×10 Thin Electric Propeller

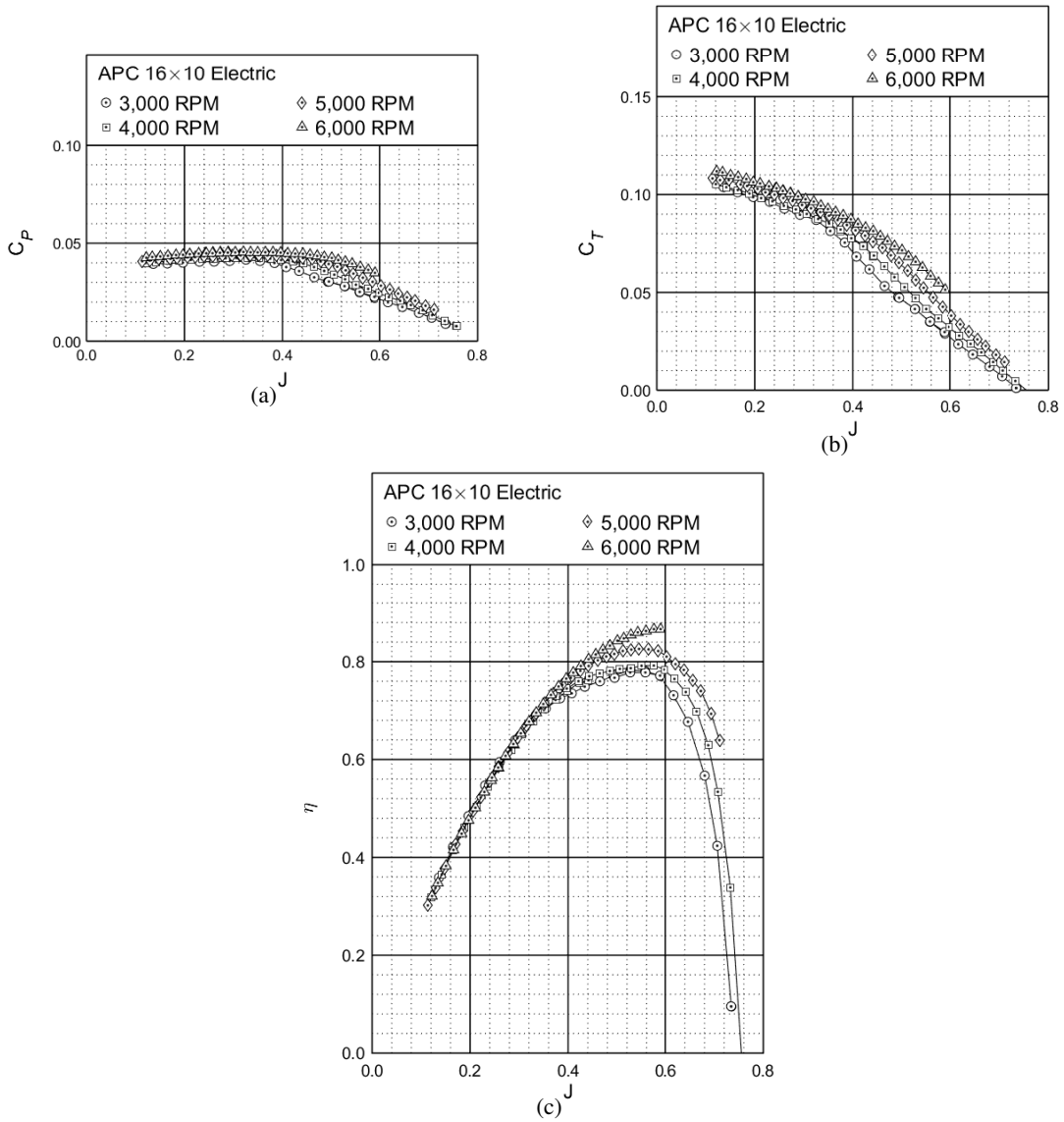

Figure 24: Performance of the APC 16×10 Thin Electric propeller: (a) thrust coefficient, (b) power coefficient, (c) efficiency.

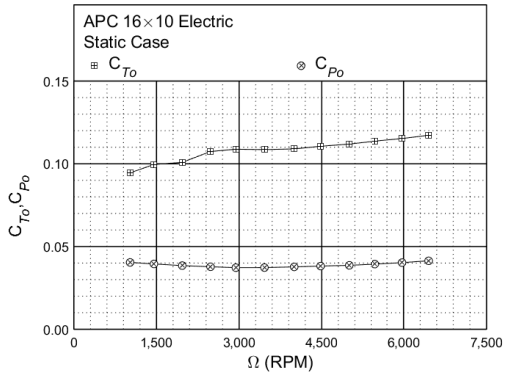

Figure 25: Static performance of the APC 16×10 Thin Electric propeller: thrust and power coefficient.

APC 16×12 Thin Electric Propeller

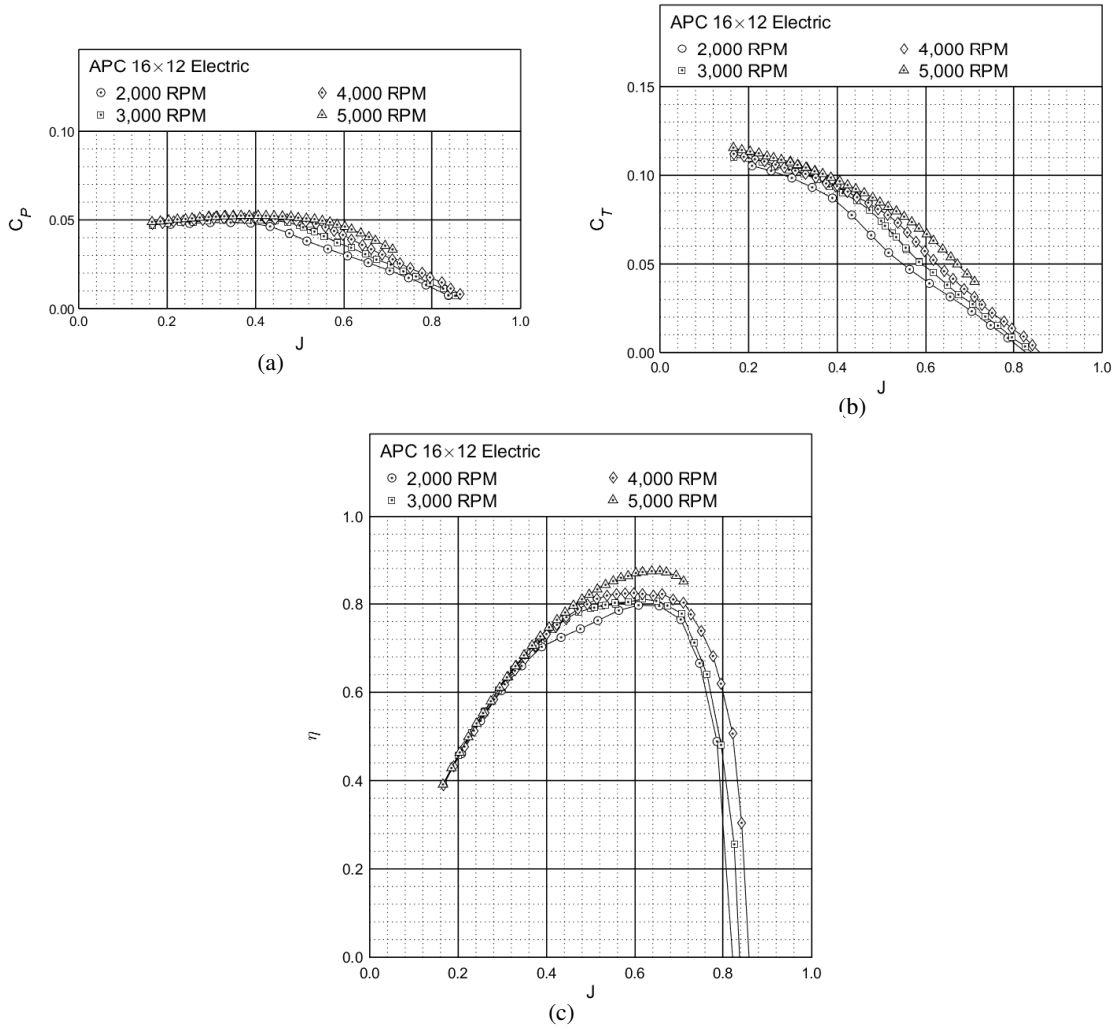

Figure 26: Performance of the APC 16×12 Thin Electric propeller: (a) thrust coefficient, (b) power coefficient, (c) efficiency.

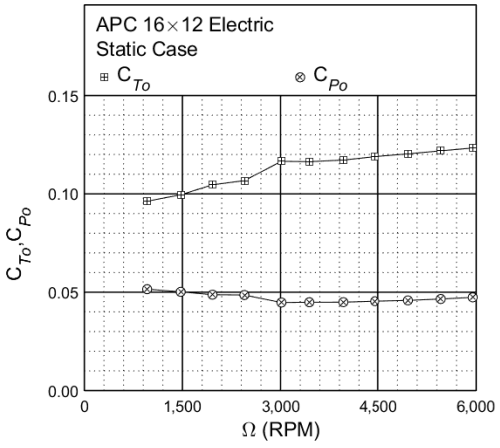

Figure 27: Static performance of the APC 16×12 Thin Electric propeller: thrust and power coefficient.

APC 18×8 Thin Electric Propeller

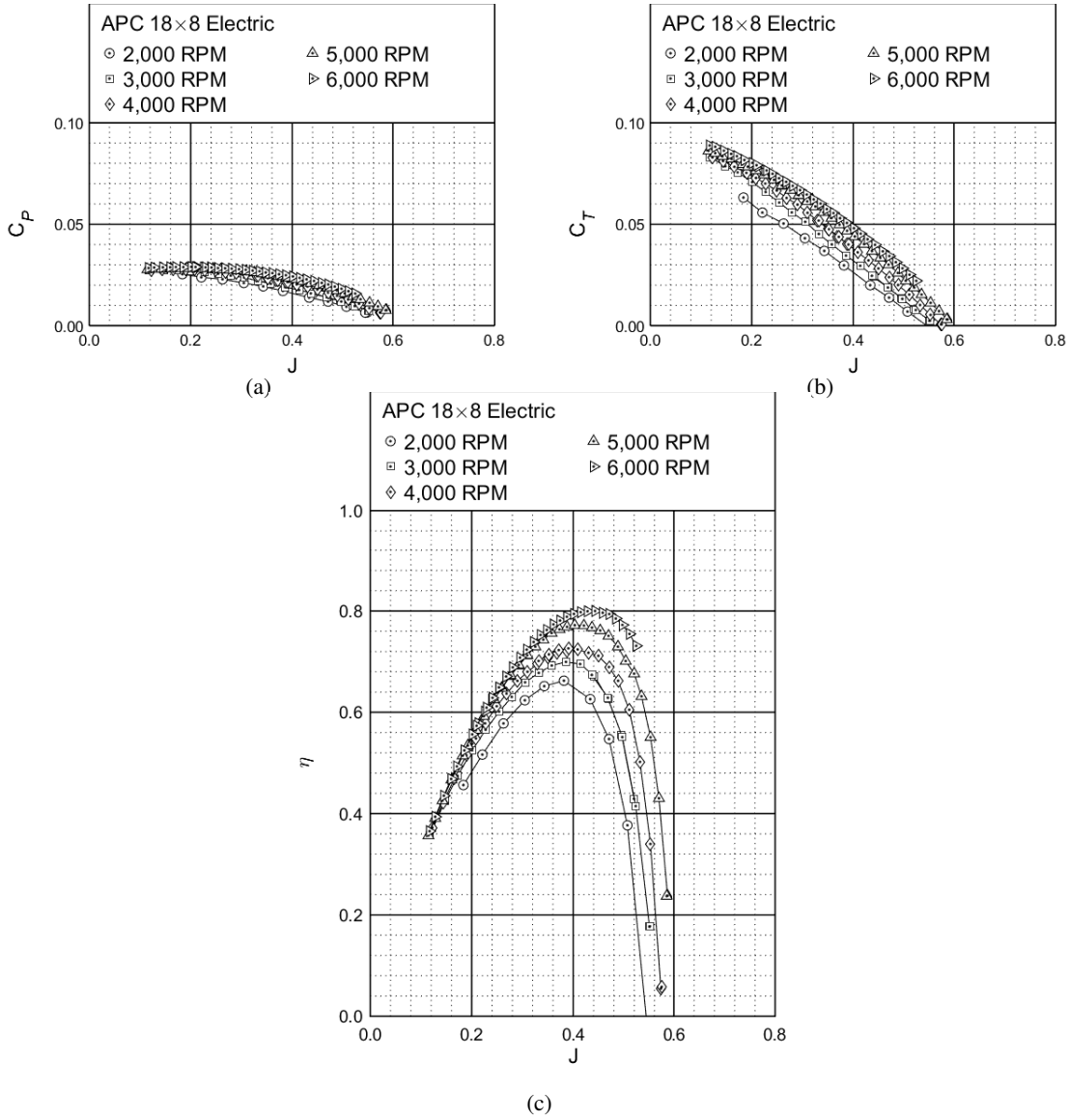

Figure 28: Performance of the APC 18×8 Thin Electric propeller: (a) thrust coefficient, (b) power coefficient, (c) efficiency.

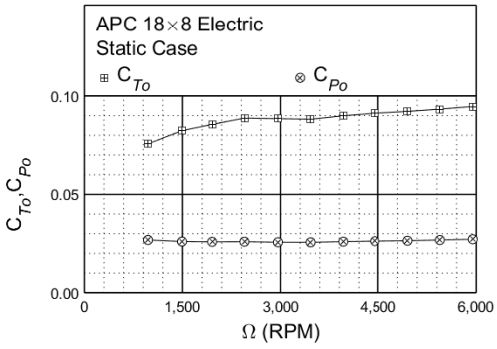

Figure 29: Static performance of the APC 18×8 Thin Electric propeller: thrust and power coefficient.

APC 18×10 Thin Electric Propeller

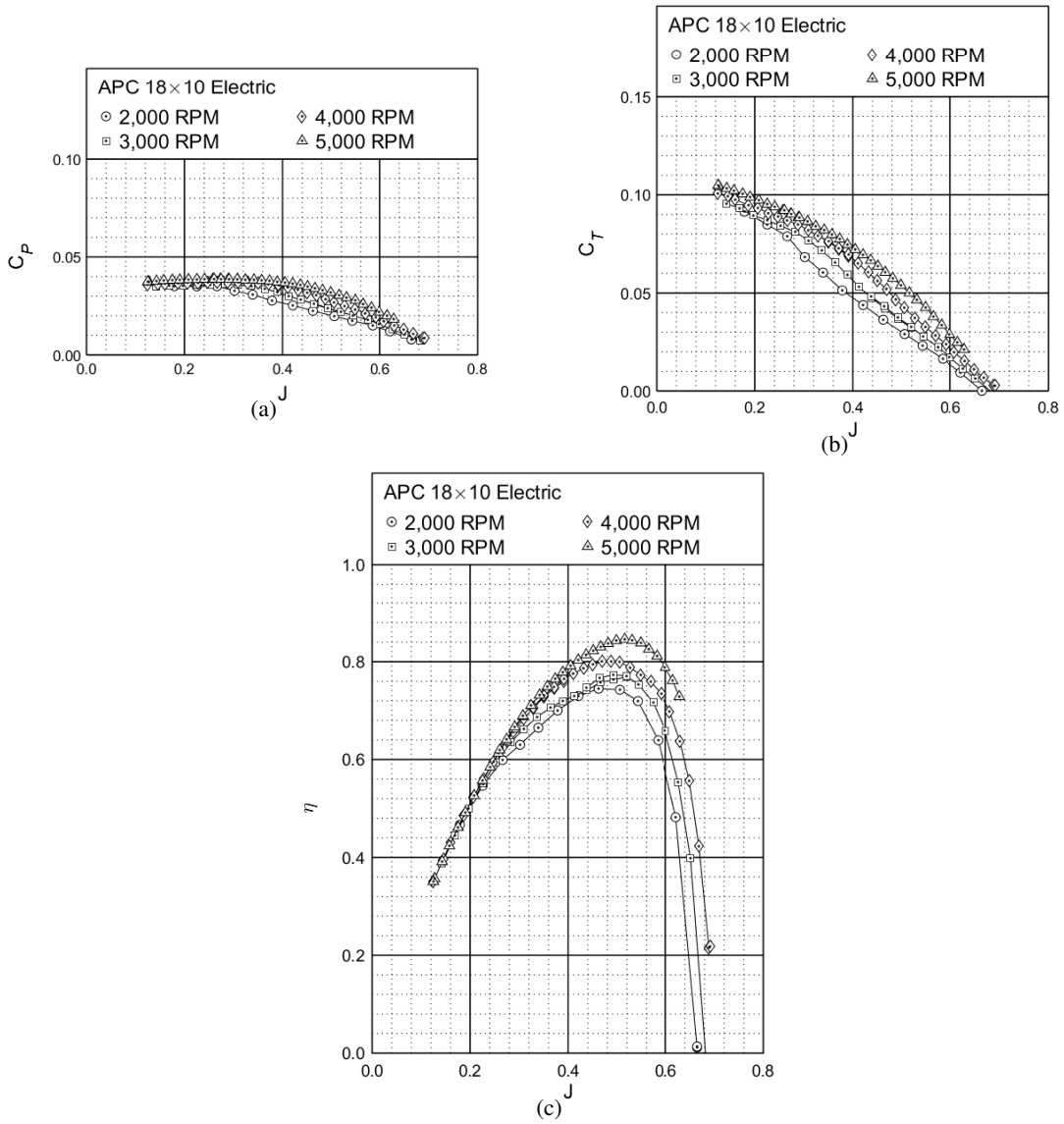

Figure 30: Performance of the APC 18×10 Thin Electric propeller: (a) thrust coefficient, (b) power coefficient, (c) efficiency.

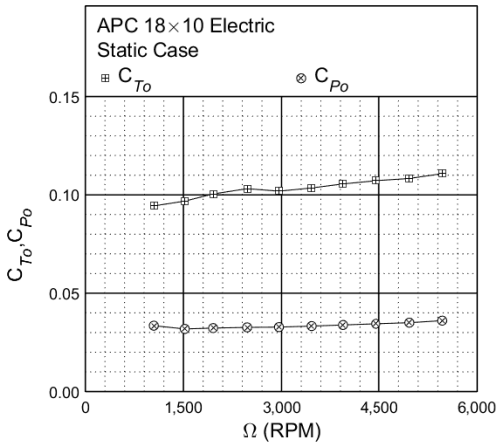

Figure 31: Static performance of the APC 18×10 Thin Electric propeller: thrust and power coefficient.

APC 18×12 Thin Electric Propeller

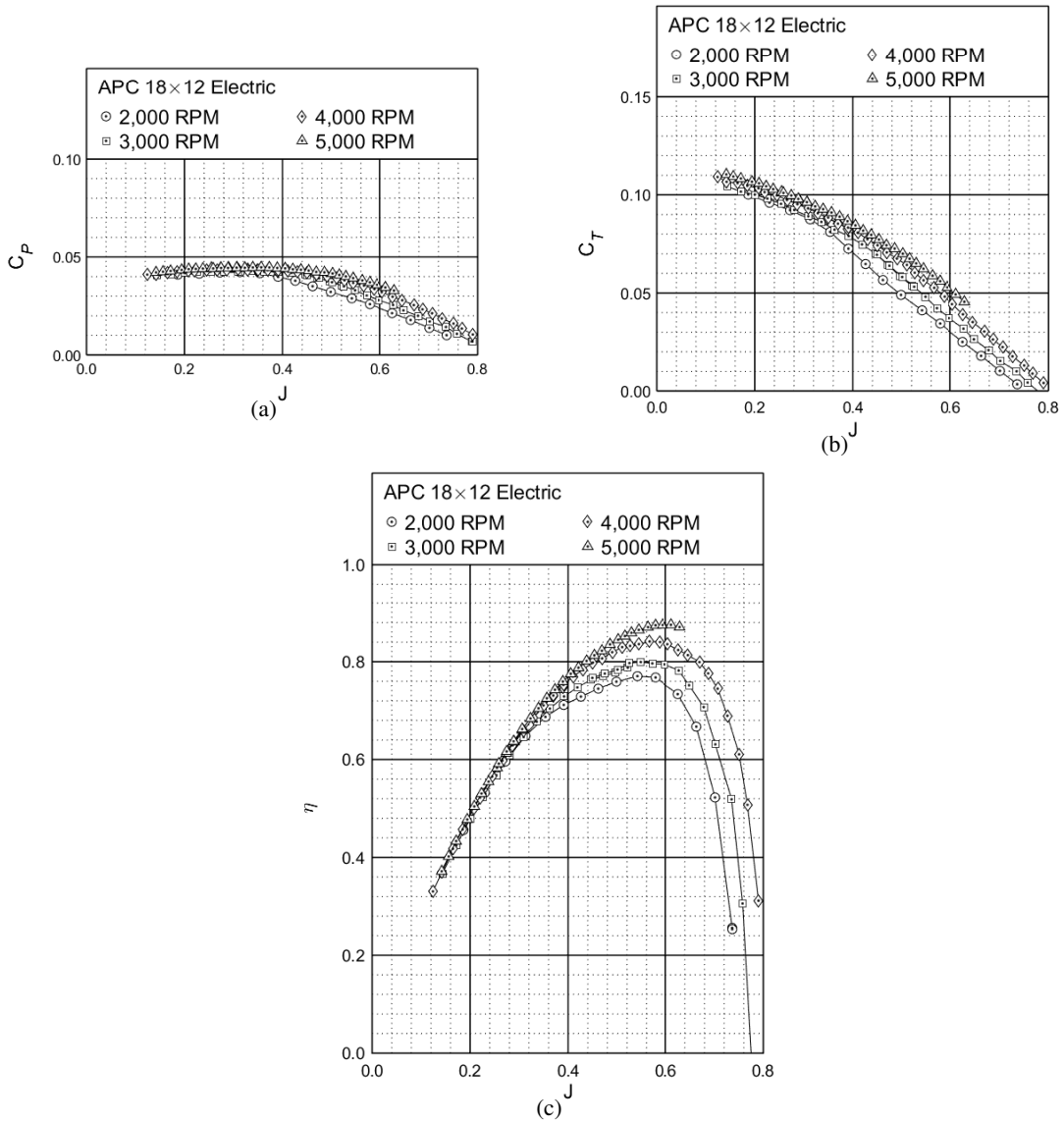

Figure 32: Performance of the APC 18×12 Thin Electric propeller: (a) thrust coefficient, (b) power coefficient, (c) efficiency.

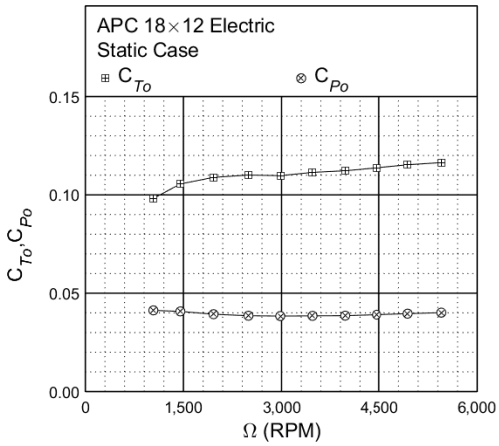

Figure 33: Static performance of the APC 18×12 Thin Electric propeller: thrust and power coefficient.

APC 20×10 Thin Electric Propeller

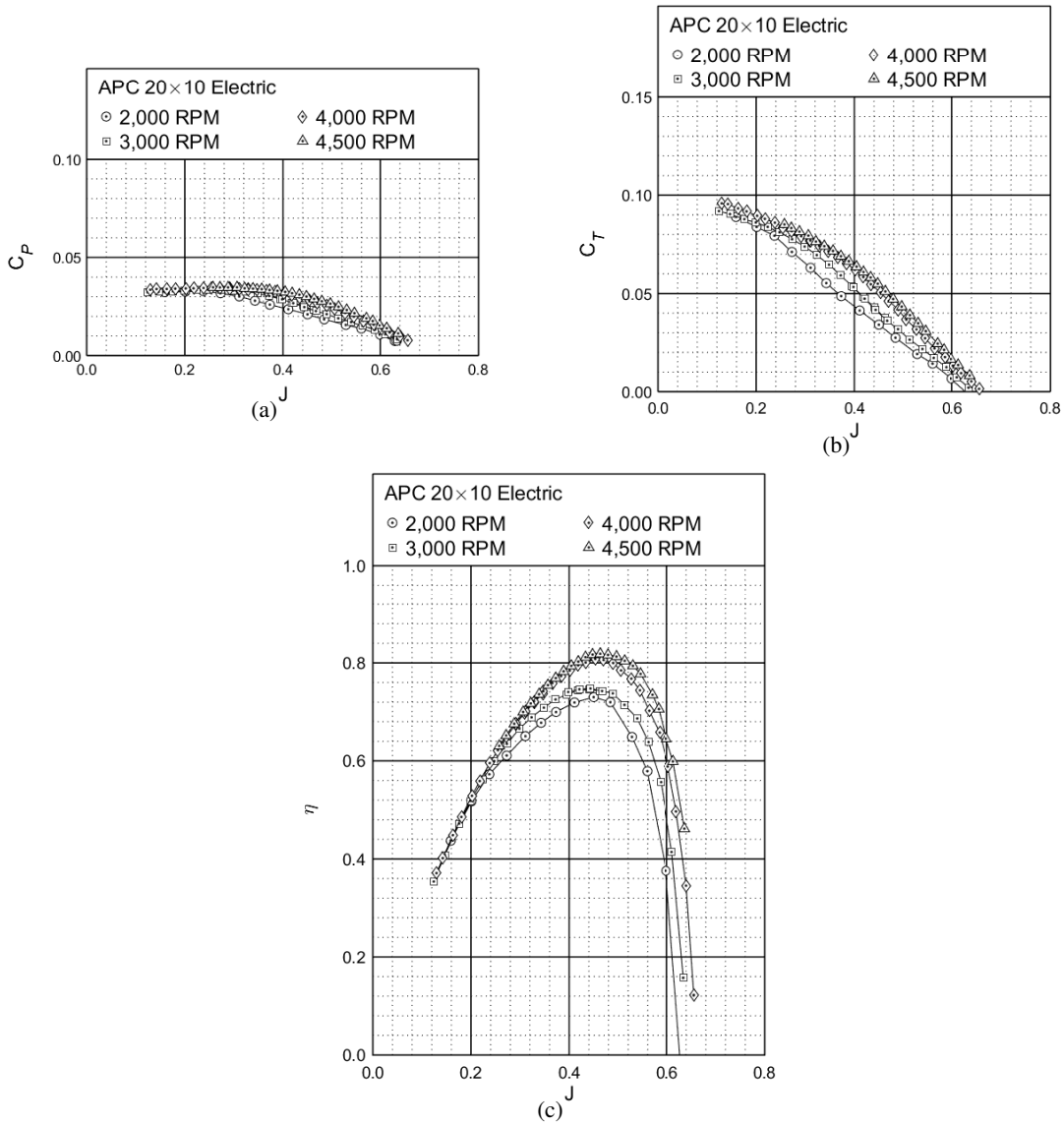

Figure 34: Performance of the APC 20×10 Thin Electric propeller: (a) thrust coefficient, (b) power coefficient, (c) efficiency.

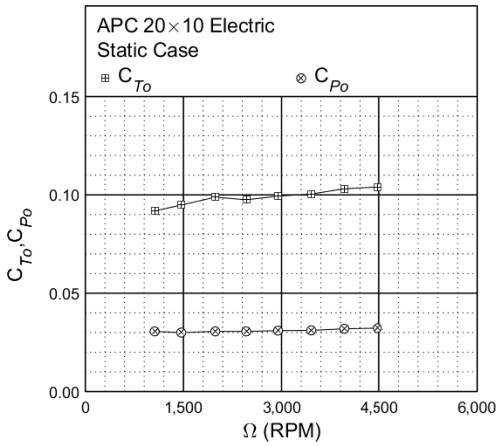

Figure 35: Static performance of the APC 20×10 Thin Electric propeller: thrust and power coefficient.

APC 21×13 Thin Electric Propeller

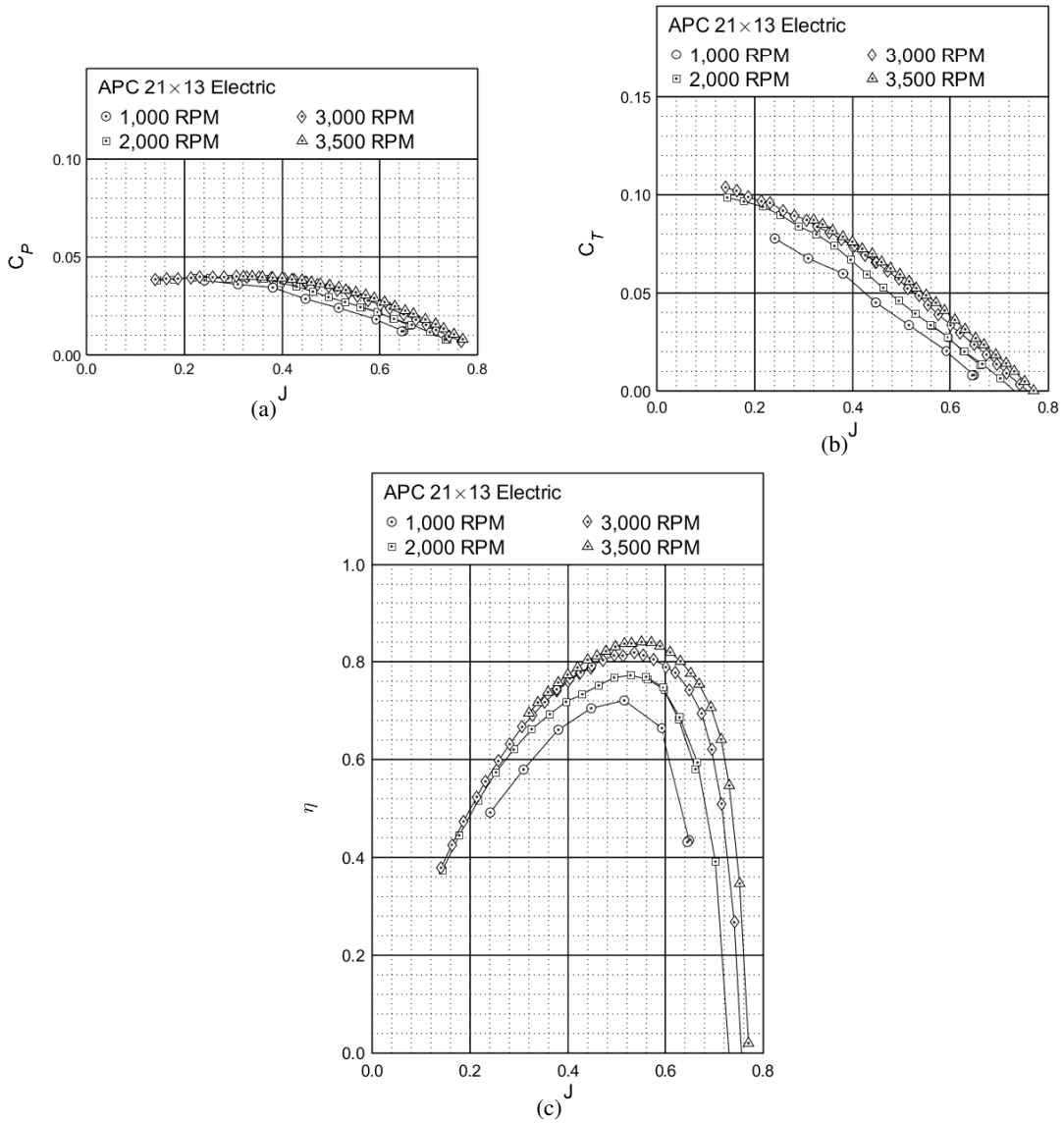

Figure 36: Performance of the APC 21×13 Thin Electric propeller: (a) thrust coefficient, (b) power coefficient, (c) efficiency.

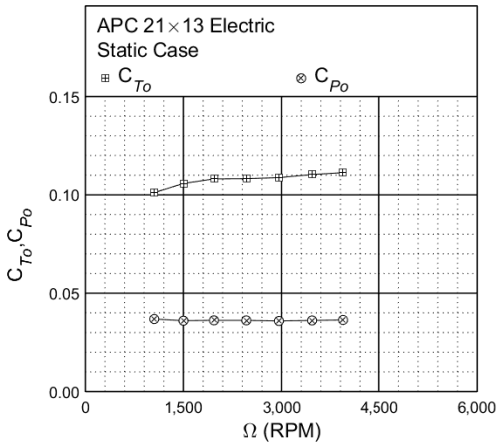

Figure 37: Static performance of the APC 21×13 Thin Electric propeller: thrust and power coefficient.

III. Summary and Future Work

This paper described the performance testing of 17 APC Thin Electric ("E") 2-bladed, fixed propellers with diameters of 12 to 21 in. with various pitch values. The propellers were tested at rotation rates of 1,000 to 7,000 RPM and advancing flows of 8 to 80 ft/s, depending on the propeller and testing equipment limitations. The motivation of this testing was to enlarge the database of publicly-available propeller performance data that could be used to optimize the propulsion system of electric unmanned aircraft. It was observed that APC-E propellers had very similar geometries among propellers of the same diameter with different pitch values, with chord remaining constant at each station while twist changes. Through performance testing it was also found that increasing the pitch of a given diameter of propeller increases the non-dimensional performance and efficiency of the propeller, while shifting these characteristics toward higher advance ratios. Similarly, for static conditions (zero velocity), increased propeller pitch increases thrust and power coefficients.

In future work, measurement of the blade geometry (chord and twist distribution) for the tested propellers will be performed, allowing Reynolds number to be estimated for the present results. The Reynolds number estimates will enable the meta-analysis of propellers currently tested with those tested in previous efforts, focusing on Reynolds number effects of APC Thin Electric propellers with identical P/D ratios. Additional future work could also include a redesign of the testing apparatus, to enable testing at higher tunnel speeds; thus, more complete performance and efficiency curves could be measured for propellers with high P/D ratios. Testing could also be expanded for other large APC Thin Electric propellers with diameters and pitch values that were not currently tested, as well as testing similarly-sized propellers from other brands.

Acknowledgments

The material presented in this paper is based upon work supported by the National Science Foundation (NSF) under grant number CNS-1646383. Marco Caccamo was also supported by an Alexander von Humboldt Professorship endowed by the German Federal Ministry of Education and Research. Any opinions, findings, and conclusions or recommendations expressed in this publication are those of the authors and do not necessarily reflect the views of the NSF.

References

[1]Dantsker, O. D., Imtiaz, S., and Caccamo, M., "Electric Propulsion System Optimization for Long-Endurance and Solar-Powered Unmanned Aircraft," AIAA Paper 2019-4486, 2019 AIAA/IEEE Electric Aircraft Technologies Symposium, Indianapolis, Indiana, Aug. 2019.

[2]Landing Products Inc., "APC Propellers," https://www.apcprop.com/, Accessed Dec. 2021.

[3]UIUC Applied Aerodynamics Group, "UIUC Propeller Data Site," https://m-selig.ae.illinois.edu/props/propDB.html.

[4]Dantsker, O. D., Caccamo, M., Deters, R. W., and Selig, M. S., "Performance Testing of Aero-Naut CAM Folding Propellers," AIAA Paper 2020-2762, AIAA Aviation Forum, Virtual Event, Jun. 2020.

[5]Brandt, J. B., *Small-Scale Propeller Performance at Low Speeds*, Master's thesis, University of Illinois at Urbana-Champaign, Department of Aerospace Engineering, Urbana, IL, 2005.

[6]Brandt, J. B. and Selig, M. S., "Propeller Performance Data at Low Reynolds Numbers," AIAA Paper 2011-1255, AIAA Aerospace Sciences Meeting, Orlando, Florida, Jan. 2011.

[7]Uhlig, D. V., *Post Stall Propeller Behavior at Low Reynolds Numbers*, Master's thesis, University of Illinois at Urbana-Champaign, Department of Aerospace Engineering, Urbana, IL, 2007.

[8]Uhlig, D. V. and Selig, M. S., "Post Stall Propeller Behavior at Low Reynolds Numbers," AIAA Paper 2008-407, AIAA Aerospace Sciences Meeting, Reno, Nevada, Jan. 2008.

[9]Lundstrom, D., *Aircraft Design Automation and Subscale Testing*, Ph.D. thesis, Linkoping University, Department of Management and Engineering, Linkoping, Sweden, 2012.

[10]Lundstrom, D. and Krus, P., "Testing of Atmospheric Turbulence Effects on the Performance of Micro Air Vehicles," *International Journal of Micro Air Vehicles*, Vol. 4, No. 2, Jun. 2012, pp. 133–149.

[11]Deters, R. W. and Selig, M. S., "Static Testing of Micro Propellers," AIAA Paper 2008-6246, AIAA Applied Aerodynamics InProceedings, Honolulu, Hawaii, Aug. 2008.

[12]Deters, R. W., *Performance and Slipstream Characteristics of Small-Scale Propelllers at Low Reynolds Numbers*, Ph.D. thesis, University of Illinois at Urbana-Champaign, Department of Aerospace Engineering, Urbana, IL, 2014.

[13]Deters, R. W., Kleinke, S., and Selig, M. S., "Static Testing of Propulsion Elements for Small Multirotor Unmanned Aerial Vehicles," AIAA Paper 2017-3743, AIAA Aviation Forum, Denver, Colorado, June 2017.

[14]Deters, R. W., Dantsker, O. D., Kleinke, S., Norman, N., and Selig, M. S., "Static Performance Results of Propellers Used on Nano, Micro, and Mini Quadrotors," AIAA Paper 2018-4122, AIAA Aviation Forum, Atlanta, Georgia, June 2018.

[15]Lindahl, P., Moog, E., and Shaw, S. R., "Simulation, Design, and Validation of an UAV SOFC Propulsion System," *IEEE Transactions on Aerospace and Electronic Systems*, Vol. 48, No. 3, Jul. 2012, pp. 2582–2593.

[16]Chaney, C. S., Bahrami, J. K., Gavin, P. A., Shoemake, E. D., Barrow, E. S., and Matveev, K. I., "Car-Top Test Module as a Low-Cost Alternative to Wind Tunnel Testing of UAV Propulsion Systems," *Journal of Aerospace Engineering*, Vol. 27, No. 6, Nov. 2014.

[17]Dantsker, O. D., Selig, M. S., and Mancuso, R., " A Rolling Rig for Propeller Performance Testing," AIAA Paper 2017-3745, AIAA Applied Aerodynamics InProceedings, Denver, Colorado, June 2017.

[18]Drela, M., "DC Motor / Propeller Matching," http://web.mit.edu/drela/Public/web/qprop/motorprop.pdf.

[19]Drela, M., "First-Order DC Electric Motor Model," http://web.mit.edu/drela/Public/web/qprop/motor1_theory.pdf.

[20]Drela, M., "Second-Order DC Electric Motor Model," http://web.mit.edu/drela/Public/web/qprop/motor2_theory.pdf.

[21]Green, C. R. and McDonald, R. A., "Modeling and Test of the Eciency of Electronic Speed Controllers for Brushless DC Motors," AIAA Paper 2015-3191, AIAA Aviation Forum, Dallas, Texas, Jun. 2015.

[22]Gong, A. and Verstraete, D., "Experimental Testing of Electronic Speed Controllers for UAVs," AIAA Paper 2017-4955, AIAA/SAE/ASEE Joint Propulsion InProceedings, Atlanta, Georgia, July 2017.

[23]Gong, A., MacNeill, R., and Verstraete, D., "Performance Testing and Modeling of a Brushless DC Motor, Electronic Speed Controller and Propeller for a Small UAV," AIAA Paper 2018-4584, AIAA Propulsion and Energy Forum, Cincinnati, Ohio, July 2018.

[24]Gong, A., Maunder, H., and Verstraete, D., "Development of an in-fight thrust measurement system for UAVs," AIAA Paper 2017-5092, AIAA/SAE/ASEE Joint Propulsion InProceedings, Atlanta, Georgia, July 2017.

[25]Khodadoust, A., "An Experimental Study of the Flowfield on a Semispan Rectangular Wing with a Simulated Glaze Ice Accretion," Ph.D. Thesis, University of Illinois at Urbana-Champaign, Urbana, IL, 1993.

[26]Anderson, J.D., Jr., *Fundamentals of Aerodynamics*, 2nd ed., McGraw-Hill, Inc., New York, 1991.

[27]Glauert, H., "Wind Tunnel Interference on Wings, Bodies and Airscrews," Aeronautical Research Committee R&M 1566, 1933.

[28]Barlow, J.B., Rae, W.H., Jr., and Pope, A., *Low-Speed Wind Tunnel Testing*, 3rd ed., John Wiley & Sons, Inc., New York, 1999.

[29]O. Dantsker and R. Mancuso and M. Vahora and M. Caccamo, "Unmanned Aerial Vehicle Database," http://uavdb.org/, Accessed Jan. 2022.